Surface Relaxation of a Hexagonal Lyotropic Mesophase

P. Lang,*,† Chr. Braun,† R. Steitz,† G. H. Findenegg,† and H. Rhan‡

Iwan-N.-Stranski Institute, Technical University Berlin, Strasse des 17. Juni 112, D−10623 Berlin, Germany, and HASYLAB at DESY, Notkestrasse 85, D−22603 Hamburg, Germany

Received: April 7, 1998

The influence of the free surface on the structure of the hexagonal lyotropic mesophase (H_1) of the binary surfactant system pentaoxyethylene-*n*-dodecylether + water was probed by grazing incidence X-ray diffraction. The reflected diffraction patterns consist of hexagonally arranged discrete spots showing that the orientation of the (01) lattice planes is parallel to the surface. This orientation extends several micrometers into the bulk. We report on experimental evidence for the coexistence of two lattices with different *d*-spacings. In the reflected diffraction patterns observed at a limited penetration depth of the incident beam, the Bragg spots split into two well-resolved peaks, one of which disappears as the penetration depth is increased. Analysis of the diffraction data reveals the existence of a surface layer of hexagonally packed micelles with a lattice constant smaller than the corresponding bulk value.

Introduction

The reduced spacial dimensionality of a surface exerts strong influence on the relative stability of different phases of a given substance and causes a wealth of surface effects on phase transitions.[1] Because the surface particles are usually less tightly bound than those in the interior of the phase, one expects that the less ordered phase is stabilized by the surface and thus the surface melts at a lower temperature than the bulk phase.[2] The opposite situation, when an ordered surface layer coexists with a disordered bulk phase, has been observed so far only for thermotropic liquid crystals[3] and, more recently, for higher *n*-alkanes[4,5] and alkanols.[6] It has been argued that this behavior is due to the rigid core and/or flexible chain geometry of these molecules and the ordering field which is exerted on such molecules by a flat surface. One may speculate that surface ordering might cause a stronger interaction and possibly a closer packing of the chains in the surface region as compared with the bulk ordered phase. In this paper we report the observation of such an effect at the free surface of a lyotropic liquid crystal formed in an aqueous system of a common nonionic surfactant.

Aqueous systems of oligo(oxyethylene)-*n*-monoalkylethers, commonly abbreviated as C_mE_n, exhibit a variety of phases in the temperature−composition plane.[7] Most members of the series with $m \geq 10$ and $n \geq 4$ form lyotropic mesophases at higher mass fractions *w* of the amphiphile.[8] In this contribution we focus on the investigation of the hexagonal phase, H_1, of the system $C_{12}E_5$ + water. This phase is believed to comprise cylindrical micelles arranged in a two-dimensional hexagonal array which is quasi infinite in the direction of the cylinder long axis. This picture is supported by the observation of tubular micelles in the isotropic L_1 phase which borders the H_1 phase.[9] According to Figure 1 the stability region of the H_1 phase of the system $C_{12}E_5$ + water spans a composition range of $0.3 \leq w \leq 0.58$ at 0 °C with a maximum melting temperature of about 24 °C at $w \approx 0.45$.[10] In a previous study we showed that the melting of the surface region of the hexagonal phase at a given composition is shifted to a slightly higher temperature compared with the bulk phase.[11] Here we address the question whether the observed surface induced shift of the $H_1 \rightarrow L_1$ phase transition temperature is connected to a variation of the liquid cristalline structure close to the surface (i.e., a surface relaxation of the H_1 phase at temperatures below its melting point). A related effect was reported by Zhou et al.[12] who showed that the structure of a microemulsion which is bicontinuous in the bulk is forced to a lamellar ordering in the surface region. However, to our knowledge no experimental evidence has been presented so far showing a similar effect on hexagonal lyotropic mesophases.

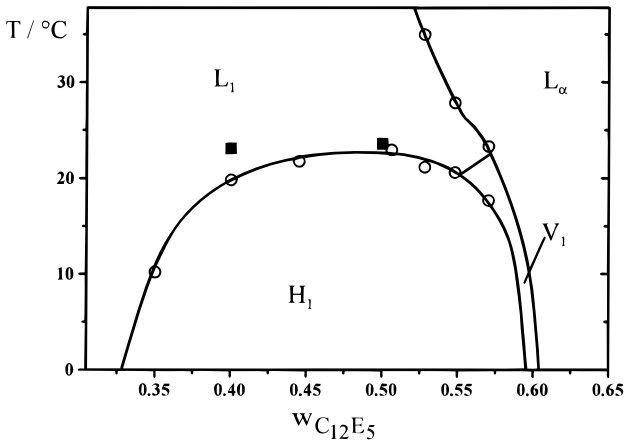

Figure 1. Part of the phase diagram of $C_{12}E_5$ + water. The isotropic micellar solution phase is denoted L_1, the lyotropic liquid cristalline phases are denoted H_1 (hexagonal), V_1 (cubic), and L_α (lamellar). The open symbols were read off graphically from ref 10; the full squares are the phase transition temperatures determined for the present samples and the full lines are guides to the eye.

An excellent tool for surface sensitive structural investigations is grazing incidence X-ray diffraction (GIXD).[14,15] The general set up for this kind of experiment is depicted in Figure 2. In contrast to a conventional small angle X-ray scattering (SAXS) experiment, the diffraction pattern is observed in reflection geometry rather than in transmission. Accordingly, the scat-

† TU-Berlin.
‡ HASYLAB at DESY.

S1089-5647(98)01756-8 CCC: $15.00
Published on Web 09/09/1998

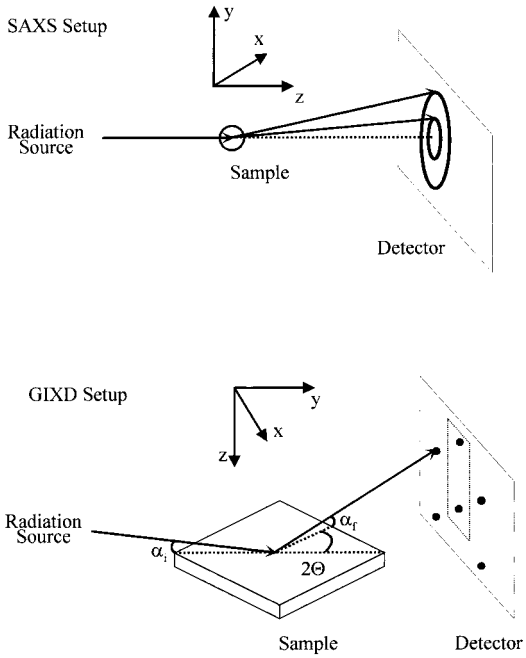

Figure 2. General set up for diffraction experiments in conventional transmission geometry (above) and in reflection geometry (below). For both set ups the *z*-direction is defined perpendicular to the sample surface but in a SAXS experiment the incident beam travels in the *z*-direction while it propagates close to the *y*-direction in a GIXD experiment. In a SAXS experiment bulk properties are probed while structural information from the bulk and the surface of the sample can be separated in a GIXD experiment applying different angles of incidence α_i.

tering vector is given by the wave vector difference of scattered and incident beam. The momentum transfer Q_z perpendicular to the reflecting surface (the *z*-direction) is given by $Q_z = 2\pi(\sqrt{\sin^2\alpha_i+\chi} + \sqrt{\sin^2\alpha_f+\chi})/\lambda$. Here λ is the X-ray wavelength, α_i is the angle of incidence, α_f is the exit angle, and χ is related to the complex index of refraction by $n = 1 - \chi/2 = 1 - \lambda^2\rho_e r_0/2\pi + i\mu\lambda/4\pi$ with $r_0 = 2.82 \times 10^{-5}$ Å being the Thompson scattering length of a single electron and μ is the linear absorption coefficient of the sample. The in-plane momentum transfer is given by $Q_{xy} = 4\pi\sin(\theta)/\lambda$ with 2θ being the angle between the projections onto the surface plane of the incident and the diffracted beam. In the experiments to be discussed below we have kept the detector (either an image plate or a position sensitive detector) at a fixed position with respect to the surface (i.e., α_f is determined by the distance of the observed peak from the sample horizon). Structural information from the sample surface region and from the bulk may be distinguished simply by variation of the angle of incidence. If α_i is smaller than α_c, the critical angle of total external reflection, the incident beam is not refracted into the sample but degenerates to an evanescent wave propagating parallel to the surface. In this case the X-rays penetrate the sample only to a limited depth Λ which is approximately $\Lambda \approx 4.6$ nm in the present case ($\Lambda = (2k\alpha_c)^{-1}$ for $\alpha_i \ll \alpha_c$ with k being the momentum of the incident wave vector).[13] On the other hand Λ extends to a macroscopic scale if α_i exceeds α_c. Therefore, structural properties of the bulk and the surface region will contribute to the reflected diffraction pattern with different weights depending on α_i.

Experimental Section

The surfactant with a purity higher than 98% was purchased by Nikko and used without further purification. As solvent we used high purity water from a Milli-Q purification system by Millipore. The mixtures were prepared by weight and kept at 25 °C at least 24 h prior to to the experiment to allow for homogenization.

The GIXD experiments were performed at the triple-axis spectrometer of beamline D 4.1 at the Hamburger Synchrotronstrahlungslabor (HASYLAB). A detailed description of the experimental set up is given elsewhere.[16,17] The resolution element of this diffractometer is 4×10^{-3} nm^{-1} in Q_x and Q_z, in Q_y (i.e., parallel to the incident beam) it is 5×10^{-4} nm^{-1}.[17] We used an image plate to map the diffraction patterns in the *xz*-plane and a position sensitve detector, PSD (OED M50 by MBraun Munich, Germany), for more quantitative investigations of the Bragg peaks in the forward ($x = 0$) direction. The wavelength λ was set to 0.133 nm, the beam was collimated to rectangular cross section by slits of 1 mm in width and 50 μm in height, and the sample to detector distance was set to 932 mm. The sample cell was designed to minimize solvent evaporation and was thermostated with an accuracy better than 0.02 K. A detailed description of the cell is given elsewhere.[11] A conventional SAXS experiment on the H_1 bulk phase was conducted as a reference with the same set up. However, the sample to detector distance was 335 mm and a quadratic beam profile of 200 μm side length (point collimation) was applied. A commercial quartz capillary (inner diameter 980 μm, wall thickness 10 μm) for use in a Kratky compact camera was used as sample cell. Complementary rocking scans were performed at the TU Berlin on a home-built reflectometer specifically designed for the investigation of liquid surfaces. This instrument operates on $\lambda = 0.154$ nm (Cu Kα), and the beam profile was chosen similar to that applied in the GIXD experiments at HASYLAB. Usually rocking scans are performed setting the reflectometer such that the specularly reflected beam coincides with a Bragg peak and then tilting the sample surface stepwise against the horizontal while the reflectometer is kept in a fixed geometry. For liquid surfaces, rocking curves have to be obtained by rocking the instrument around the sample (i.e., scanning α_i while the sample position and the angle between incident and reflected beam ($180° - (\alpha_i + \alpha_f)$) are fixed).

Results and Discussion

Alignment of the Lattice Planes by the Surface. In the GIXD experiments two samples of $C_{12}E_5 + H_2O$ with different compositions (surfactant mass fraction $w = 0.39$ and $w = 0.49$, respectively) were investigated. The corresponding phase transition temperatures $T_{H_1 \to L_1}$ were found to be 23.1 ± 0.1 °C and 23.6 ± 0.1 °C, respectively. Bragg peaks of the hexagonal phase first occur at these temperatures upon stepwise cooling in steps of 0.1 K. The transition temperatures are for both sample compositons slightly higher than reported in literature.[10] For the scattering experiments the temperature was set 0.5 K below the respective transition temperatures. Image plates of a SAXS and a GIXD experiment on a sample with $w = 0.39$ are shown in Figure 3. The transmitted diffraction pattern (SAXS) consists of Debye−Scherrer rings the radii of which are related by the ratio $1:\sqrt{3}$ as expected for a powder sample with hexagonal symmetry. The reflected diffraction pattern (GIXD), on the other hand, consists of a distinct set of hexagonally arranged Bragg peaks.

Hexagonal diffraction patterns like the one displayed in Figure 3 are generated by a regular arrangement of cylindrical micelles

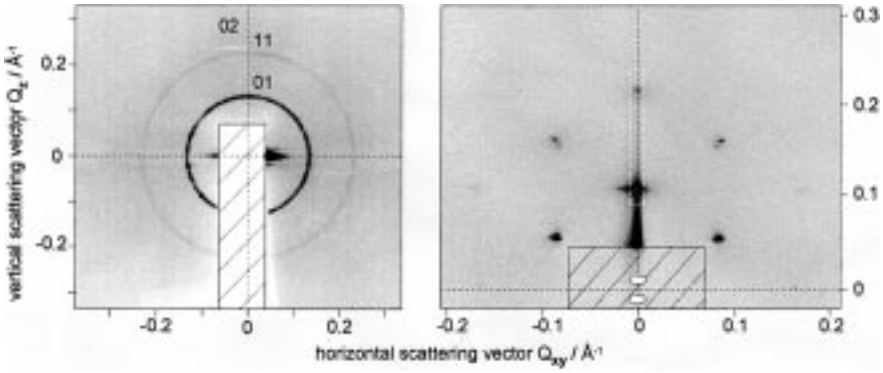

Figure 3. Image plates of the diffraction patterns from the H_1 phase of $C_{12}E_5$ + water at a surfactant weight fraction of $w = 0.39$. The SAXS pattern (left) recorded in transmission geometry consists of Debye-Scherrer rings with a ratio of scattering vectors $Q_2/Q_1 = \sqrt{3}$. In contrast, the GIXD (right) pattern recorded at $\alpha_i = 0.8\alpha_c$ consists of hexagonally arranged discrete spots, which split into well resolved doublets of peaks if $\alpha_i \leq \alpha_i$. The hatched areas in both pictures are beam stops and the white ovals on the beam stop of the GIXD image plate represent the positions of the primary and the specularly reflected beam respectively. The white dashed rectangle represents the location of the position sensitive detector used to obtain the spectra shown in Figure 5.

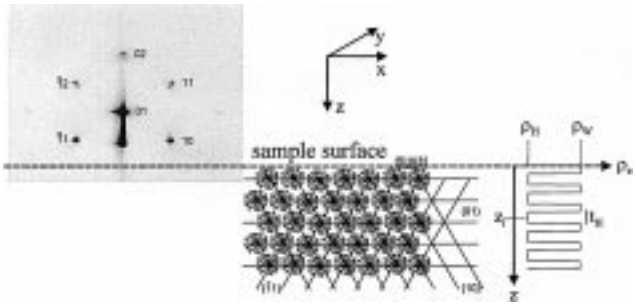

Figure 4. Reflected diffraction pattern of the H_1-phase of $C_{12}E_5$ + water at a surfactant weight fraction of $w = 0.39$ together with a sketch of the corresponding hexagonal packing of micelles in real space. The long axis of the cylindrical micelles is perpendicular to the paper plane and parallel to the incident beam which propagates in the *y*-direction. On the far right the electron density profile perpendicular to the surface is sketched which was used for the simulation of scattering curves.

in the liquid sample, as sketched in Figure 4. Threadlike micelles are oriented with their long axes parallel to the surface. They form hexagonally packed bundles in the plane perpendicular to their long axis (*xz*-plane) with sets of nearest-neighbor lattice planes, (01), parallel to the liquid/air interface. This regular two-dimensional packing of the micelles gives rise to the two-dimensional diffraction pattern observed with the 01 and 02 Bragg spots located in the beam-forward direction as a function of momentum transfer Q_z only. No other orientation of the hexagonal arrays with respect to the liquid/air interface is realized. Any inclination of the lattice planes i.e., any rotation ϕ of the arrays around the *y*-axis would rotate the corresponding diffraction pattern by ϕ as well and thus cause arching of the Bragg spots. In the limiting case of a uniform distribution of ϕ, diffraction rings would occur which are not observed in our GIXD experiments. Further information on the orientation of (01) lattice plane with respect to the surface was obtained from rocking scans. If the sample were perfectly single crystalline in the *z*-direction, with the 01 lattice planes parallel to the surface, the Bragg condition could be met only if $\alpha_i = \alpha_f$. Thus, tilting the sample against the horizontal (or in our case rocking the diffractometer around the sample) would lead to a complete loss of scattered intensity and a plot of the scattered intensity versus the rocking angle (a so-called transverse rocking curve) would result the Dirac δ-function or better in a resolution limited Gaussian for a real diffractometer. On the other hand, if the lattice planes are randomly inclined with respect to the horizontal, rocking of the sample (here the diffractometer) will not lead to a complete loss of scattered intensity, because there will always be sets of lattice planes which fulfil the Bragg condition. The shape of the rocking curve therefore directly reflects the distribution of inclination angles ϕ. Shortly after cooling the sample to 0.5 K below the $T_{L_1 \rightarrow H_1}$ transition temperature, the experimental rocking curves are Gaussian with a full width at half-maximum (fwhm) of 0.03°. However, we observed a broadening of the rocking curves up to the tenfold of the initial fwhm on a time scale of days. We attribute this broadening to an increasing macroscopic surface roughness which inevitably develops when the sample transforms from L_1 to H_1 on cooling and thus causes the *xy*-plane and the surface plane to become locally different. The rocking curves have to be recorded at the peak position, i.e., $\alpha_i \approx 5\alpha_c$, in the present case which corresponds to a penetration depth of the X-rays of several micrometers. This implies that the rocking curves represent the distribution of inclination angles ϕ down to a depth of some micrometers. In other words, even deep in the bulk the (01) lattice planes are inclined less than 0.03° initially and less than 0.3° after annealing with respect to the surface plane.

In a GIXD experiment the incident beam propagates essentially in the *y*-direction. Thus, by mapping the *xz*-plane with an image plate, only those sets of lattice planes which fulfill the Bragg condition will be detected. Rotation of the sample around the *z*-axis did not change the diffraction pattern indicating that all inclinations of the cylinder long axis with respect to the beam forward direction are equally distributed, and only domains oriented to meet the Bragg condition contribute to the scattering. This finding is in agreement with the result of the transmission diffraction experiment. In the SAXS experiments the primary beam is incident perpendicular to the sample surface (i.e., in the *z*-direction). Mapping the *xy*-plane with an image plate will result in Debye−Scherrer rings of scattered intensity if the sample is polycrystalline in this plane. As to be seen from Figure 3, such rings are indeed observed, with a ratio of the momentum tranfers $Q_2/Q_1 = 1.73$, which is typical for hexagonal structures. In conclusion, these findings show that in the region monitored by GIXD the sample is polycrystaline in the *xy*-plane but in the direction perpendicular to it the sample is quasi monocrystaline with a maximum deviation of the (01) lattice plane from the horizontal of about 0.3°.

Formation of a Surface Lattice. Closer inspection of the grazing incidence diffraction patterns reveals that the Bragg spots consist of doublets of peaks, if observed at $\alpha_i \leq \alpha_c$ (see Figure 3, right), indicating the existence of two distinct

hexagonal lattices in real space. This effect was investigated quantitatively by recording spectra of the 01 spot for various α_i with a position-sensitive detector (PSD) fixed at the position indicated by the dashed rectangle in Figure 3. With this geometry the experiment probes only electron density variations along the direction perpendicular to the surface, because the scattered intensity is a function of *z*-component of the scattering vector Q_z alone. The doublet patterns remain unchanged when moving the sample in the *xy*-plane or rotating the sample around its *z*-axis. However, the relative intensity of the two peaks of each doublet changes in a systematic manner as the angle of incidence is varied. With increasing α_i the Bragg spot at larger Q_z of each doublet becomes less prominent and eventually vanishes. Because an increase of the angle of incidence causes a drastic increase in penetration depth of the X-rays, the Bragg spots at larger Q_z have to be ascribed to a structure which is not present in the bulk sample. This assignment is consistent with the finding that the rings observed in the transmitted small angle scattering pattern do not exhibit a doublet character. The fact that the peak representing the bulk lattice is still visible at $\alpha_i \leq \alpha_c$ can be attributed to the macroscopic surface roughness which inevitably develops at the free surface of the H_1-phase. Due to this increased surface roughness the angle of incidence is no longer well defined on a microscopic scale and the effective penetration depth is therefore larger than implied by the angle α_i which is experimentally preset. This observation is well in line with the observed broadening of the rocking curves as described above.

The experimental PSD spectra can be described phenomenologically by a sum of a Gaussian and a Lorentzian profile superimposed on an exponentially decaying background.

$$I(Q_z) = \frac{A_G}{\sigma\sqrt{\pi/2}} \exp\left\{-\frac{2(Q_z - C_G)^2}{\sigma^2}\right\} + \frac{2A_L\xi}{\pi(\xi^2 + 4(Q_z - C_L)^2)} + B\exp\left\{-\frac{Q_z}{\tau}\right\} \quad (1)$$

Here A_G, C_G, and σ are the area, the center position, and the fwhm of the Gaussian while A_L, C_L, and ξ are the corresponding parameters for the Lorentzian. The exponential decay is defined by B and τ. The complete set of the data obtained from the sample at a surfactant content of $w = 0.49$ together with the best fits are plotted in Figure 5 and the values of the parameters in eq 1 are collected in Table 1.

In the fitting procedure we used $Q_z = 2\pi \sin((\alpha_i + \alpha_f)/2)/\lambda$ for the momentum transfer which neglects refraction. Therefore the positions of the peaks are shifted toward higher Q_z-values and their separation decreases as the angle of incidence increases. Because refraction becomes less important at large α_i, the Bragg spacings corresponding to the data obtained at $3\alpha_c$ are physically realistic. This is confirmed by the SAXS experiment which yielded d_{SAXS} 51.18 Å for the sample at a surfactant weight fraction of $w = 0.39$. The areas of both peaks increase with α_i and the relative intensities of the peaks represented by the ratio A_G/A_L change drastically with the penetration depth of the X-ray beam. As long as α_i is smaller than the critical angle of total external reflection, the Lorentzian peak is about twice as intense as the Gaussian. For $\alpha_i > \alpha_c$, the Gaussian peak becomes more and more prominent and the ratio of the intensities eventually tends to a limiting value $A_G/A_L \approx 1.5$. On the other hand, the fwhm of the peaks does not change systematicaly with the angle of incidence. These

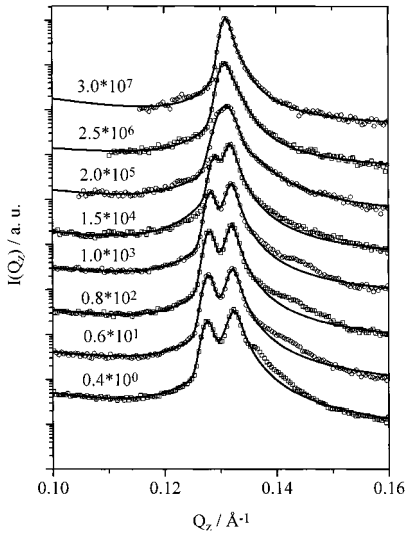

Figure 5. PSD spectra of the 01-peak of the H_1 phase of $C_{12}E_5$ + water at a surfactant weight fraction of $w = 0.49$. The detector was located at the position indicated in Figure 3. The symbols are experimental data and the full lines are fits by eq 1. The numbers above the curves indicate the multifolds of α_c at which the data were recorded multiplied with the factors used to shift the curves on the ordinate.

observations imply that an increasing number of scatterers contributes to the constructive interference as α_i is increased but the microscopic positional correlations are independent of the dimension of the scattering volume probed.

Because the observed scattering functions represent a Fourier transform of the electron density distribution of the sample (i.e., the lattice in real space) the basic features of the real-space lattice may be deduced from the applied fitting function. This is particularly simple in the present case, becasuse the Fourier transform of a Lorentzian is an exponential and the Fourier tranform of a Gaussian is again a Gaussian. We thus conclude that the observed scattering functions are generated by two coexisting lattices, one with an exponential decay in positional correlation as a function of distance, the other with a Gaussian distribution of correlation lengths. We find that the Lorentzian peak is prominent at small α_i i.e., small penetration depth, and the Gaussian becomes predominant with increasing angle of incidence, while the full width at half-maximum values of both peaks is nearly independent of α_i. This observation can be explained qualitatively by a model of a lattice with an exponential decay of the positional correlation which is present only in a surface layer with finite thickness and a two-dimensional powder of domains of a hexagonal structure with a Gaussian distribution of domain sizes in the bulk. The d-spacings for the bulk d_B and the surface lattice d_S listed in Table 1 are calculated from the respective peak positions in the diffraction pattern by Bragg's equation, viz., $d_S = 2\pi/C_L$ and $d_B = 2\pi/C_G$. The scattering signal originating from the surface layer can not be detected in the transmission SAXS experiment, because in such an experiment the angle of incidence is 90°. Consequently, the intensities of the peaks are approximately proportional to the sample thickness and the thickness of the surface layer respectively. If we take $t_S \approx 2\pi/\xi$ as a rough measure for the thickness of the surface layer, we estimate the intensity of the bulk signal to be about 10^4 times the intensity of the surface signal for our SAXS experiment.

To cross check the consistency of this model, scattering functions were simulated on the basis of a model electron density profile $\rho_e(z)$ perpendicular to the surface aimed to model

TABLE 1: Parameters of the Best Fits by Equation 1 to the PSD Spectra of the 01 Peak of the H_1-Phase of $C_{12}E_5$ + Water at Surfactant Weight Fractions of $w = 0.39$ and $w = 0.49$, Respectively[a]

α_i/α_c	A_G	$\sigma/\text{Å}^{-1}$	$C_G/\text{Å}^{-1}$	A_L	$\zeta/\text{Å}^{-1}$	$C_L/\text{Å}^{-1}$	w	$d_B/\text{Å}$	$d_S/\text{Å}$	d_S/d_B
0.4	33.86	1.15×10^{-3}	0.1218	79.58	2.26×10^{-3}	0.1258	0.39	51.56	49.90	0.97
0.6	73.81	8.82×10^{-4}	0.1217	112.43	3.28×10^{-3}	0.1253	0.39	51.59	50.12	0.97
0.8	110.88	7.69×10^{-4}	0.1218	189.46	4.01×10^{-3}	0.1250	0.39	51.56	50.25	0.97
1.0	184.27	7.61×10^{-4}	0.1220	264.16	4.65×10^{-3}	0.1249	0.39	51.48	50.27	0.98
1.5	398.65	7.61×10^{-4}	0.1224	410.93	4.34×10^{-3}	0.1249	0.39	51.32	50.27	0.98
2.0	512.25	7.39×10^{-4}	0.1225	418.23	3.77×10^{-3}	0.1247	0.39	51.25	50.36	0.98
2.5	585.08	7.00×10^{-4}	0.1227	406.82	3.34×10^{-3}	0.1246	0.39	51.19	50.42	0.98
3.0	569.99	6.62×10^{-4}	0.1229	434.75	2.93×10^{-3}	0.1245	0.39	51.10	50.45	0.99
0.4	38.08	8.29×10^{-4}	0.1277	134.78	2.44×10^{-3}	0.1324	0.49	49.19	47.43	0.96
0.6	40.96	8.27×10^{-4}	0.1278	103.16	2.16×10^{-3}	0.1322	0.49	49.13	47.51	0.97
0.8	37.26	8.00×10^{-4}	0.1280	90.24	1.98×10^{-3}	0.1320	0.49	49.06	47.57	0.97
1.0	25.59	7.48×10^{-4}	0.1282	79.39	2.09×10^{-3}	0.1320	0.49	48.98	47.59	0.97
1.5	11.97	6.70×10^{-4}	0.1289	61.78	2.16×10^{-3}	0.1317	0.49	48.72	47.68	0.98
2.0	39.10	1.36×10^{-3}	0.1310	14.81	7.56×10^{-3}	0.1336	0.49	47.96	47.01	0.98
2.5	22.02	8.89×10^{-4}	0.1307	17.22	3.37×10^{-3}	0.1325	0.49	48.05	47.40	0.99
3.0	18.95	7.49×10^{-4}	0.1310	12.39	3.28×10^{-3}	0.1323	0.49	47.96	47.46	0.99

[a] The corresponding Bragg spacings for the bulk and the surface lattice and their ratio are listed in the last three columns.

alternating slabs of hydrocarbon and aqueous ethyleneoxide layers. In the model the thickness of the hydrocarbon layer, $t_H = 33.1$ Å, was held fixed at twice the length of the all-trans length[18] of a dodecyl chain $l_c = (12 \times 1.25 + 1.54)$ Å, while the thickness of the aqueous layer t_W was allowed to attain different values in the bulk and in a region close to the surface. This leads to different lattice constants for the surface region (d_s) and for the bulk (d_b). The model electron density profile $\rho_e(z)$ is then defined in terms of a succession of box functions $\rho(z_j)$ which are centered at the nominal positions z_j of the hydrocarbon layers, viz.,

$$\rho(z_j) = \begin{cases} \rho_H, & \text{for } z_j - t_H/2 \le z \le z_j + t_H/2 \\ \rho_W, & \text{for } z_j + t_H/2 < z < z_{j+1} - t_H/2 \end{cases} \quad (2)$$

with $z_0 = 0$. Here ρ_H denotes the electron density of the hydrocarbon layer and ρ_W a mean electron density of the hydrated oxyethylene chains and water. It is assumed that the first N_S layers next to the surface have a constant spacing d_S, such that $z_j = z_{j-1} + d_S$, beyond this surface region the lattice constant is allowed to relax with the rate Γ to the bulk value by

$$z_j = z_{j-1} + d_B - (d_B - d_S) \exp\left\{\frac{N_S - j}{\Gamma}\right\} \quad (3)$$

For such an electron density profile the scattering function $S(Q_z)$ can be written as the following Fourier transform:

$$S(Q_z) = \int_{-\infty}^{\infty} \rho(z) e^{-iQ_z z} dz = \rho_H \int_0^{t_H/2} e^{-iQ_z z} dz + \rho_W \int_{t_H/2}^{z_1 - t_H/2} e^{-iQ_z z} dz + \sum_{j=1}^{\infty} \left(\rho_H \int_{z_j - t_H/2}^{z_j + t_H/2} e^{-iQ_z z} dz + \rho_W \int_{z_j + t_H/2}^{z_{j+1} - t_H/2} e^{-iQzz} dz\right) \quad (4)$$

which can be solved analytically. To account for the Gaussain size distribution of the grains in the bulk sample, we introduce a Gaussian weighting function $w(z_{jk})$ into eq 4 which describes the probability for the jth hydrocarbon layer to be located at the position $z_j = z_k + (k - j)d_b$. Because $w(z_{jk})$ depends on the distance between two locii j and k, it has to be convoluted with the electron density function $\rho_e(z)$ and the result has to be Fourier transformed to obtain the final expression for the scattered amplitude. According to the convolution theorem, this is equal to first Fourier transform both functions and subsequently multiply the the transforms. Thus the scattering function is given by

$$S(Q_z) = \frac{1}{iQ_z} \sum_{j=1}^{N} \left(\sum_{k=1}^{N_S} \rho_H \beta_H(z) + \rho_W \beta_W(z) + \sum_{k=N_S+1}^{N} P(z_{jk})(\rho_H \beta_H(z) + \rho_W \beta_W(z))\right) \quad (5)$$

with

$$\beta_H(z) = e^{-iQ_z(z_k - t_H/2)} - e^{-iQ_z(z_k - t_H/2)}$$

and

$$\beta_W(z) = e^{-iQ_z(z_k + t_H/2)} - e^{-iQ_z(z_{k+1} - t_H/2)}$$

The expression $P(z_{jk}) = \exp\{-(|j - k|d_b\sigma)^2/2\} \exp\{-iQ_B|j - k|\}$ is the Fourier tranform of $w(z_{jk})$ with Q_B being the Bragg position of the peak generated by the bulk lattice. The scattered intensity is finally obtained as the momentum square of the scattering function.

It was not possible to obtain quantitative fits by eq 5 to the experimental data, simply because the numerics are extremely time consumptive. However, the basic feature of the experimental curve should be reproduced, if the model electron density leading to eq 5 decribes the structure perpendicular to the surface of the hexagonal H_1-phase qualitatively correct. The input values for the model calculations were therefore chosen to be as close as possible to the conditions applied in the experiment. The electron density of the aqueous layers was set to the bulk value of water (i.e., $\rho_W = 0.334$ Å^{-3}), and for the hydrocarbon layers we used the bulk value of dodecane $\rho_H = 0.260$ Å^{-3}. In order to obtain two distinct peaks at small α_i in the simulation, it was necessary to set the number of slabs in the surface layer $N_S = 30$ at least. The total number of slabs was $N = 1000$ which corresponds roughly to the penetration depth of the X-ray beam at $\alpha_i = 3\alpha_c$ in the experiment. For the calculations of z_j according to eq 3, the lattice constants from the entry for $\alpha_i = 3\alpha_c$ and $w = 0.49$ in Table 1 were used. The relaxation rate from the surface spacing to the bulk value in eq 3 was chosen $\Gamma = 30$ slabs which corresponds roughly to $2\pi/\xi$. In the simulation we used the complex notation of the scattering vector depending on the mean electron density of the sample which was calculated from ρ_W and ρ_H weighted by their corresponding

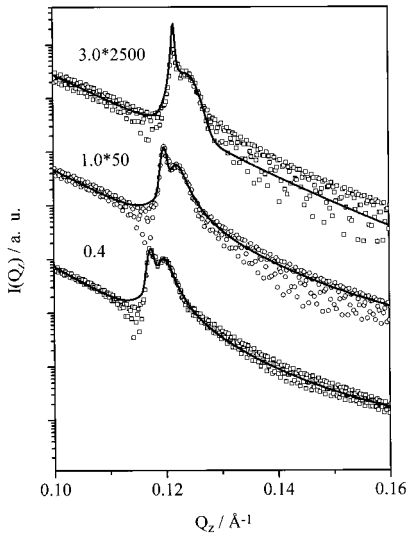

Figure 6. Scattering curves calculated from eq 5. The symbols are data simulated by the model described in the text and the full lines represent a phenomenological description by eq 1. For the sake of clarity the curves are shifted on the ordinate by appropriate factors. The numbers above the curves indicate the multifolds of α_c applied in the calculation multiplied with the factors used to shift the curves on the ordinate. The high-frequency oscillations in the simulated scattering curves are due to termination effects of the Fourier transformation.

volumes to yield $\rho_e = 0.272$ Å^{-3} and on the linear absorption coefficient for which we used the bulk value of water $\mu = 7.5$ cm^{-1}.

The results of these calculations are displayed in Figure 6 in terms of $I(Q_z)$ versus Q_z curves. Although the calculated scattering curves differ in details from the experimental data, the basic features of of the experimental data are clearly reproduced. (i) The line shapes are the same as those in the experimental data, (i.e., the curves can be phenomenologically described by the superposition of a Gaussain and a Lorentzian superimposed on an exponential background with the Lorentzian occuring at higher scattering vectors than the Gaussian). (ii) The position of the peaks is shifted to higher Q_z, and their separation decreases slightly as the angle of incidence is increased. (iii) At angles of incidence smaller than α_c, there are two well-resolved peaks with about the same intensity but with increasing α_i the peak at lower Q_z becomes increasingly prominent. We are therefore confident that the simple slab model we used for the simulation decribes the structure perpendicular to the surface of the hexagonal H_1-phase qualitatively correct.

Conclusion

In the present contribution we have shown that the ordering field of the flat surface exerts an influence on the H_1 phase of $C_{12}E_5$/water in a 2-fold way. First, the flat surface forces the hexagonal arrays to align such that the (01) lattice planes are parallel to the surface while the micellar long axes are oriented randomly in the surface plane. The maximum deviation of the (01) planes from the horizontal was observed to be about 0.3°. It is evident that this orientation persists to macroscopic scale as the reflected diffraction patterns consist of hexagonally arranged Bragg spots even if bulk properties are probed. Secondly, the free surface causes the formation of a layer containing a hexagonal lattice with a packing density of the cylindrical micelles larger than in the bulk. Although related effects are known for a variety of systems, this is the first time experimental data is presented which prove a surface relaxation in lyotropic liquid crystalline phases. The Bragg spacing of the surface lattice was found to be about one percent smaller than the spacing of the bulk lattice. However, at present it is not possible to give a reliable value for the thickness of the surface layer. A rough estimate may be obtained from simulated scattering curves based on a simple slab model. These suggest the surface lattice has to comprise at least 30 layers, to account for the observed diffraction patterns. To date we do not have a physical explanation for the observed shrinkage of the lattice close to the surface. One might speculate that the surface energy is lowered the more densely micelles are packed in the first layer and that the hexagonal arrays in the layers below have to match the geometric constraints set by the first layer. This picture would suggest that the occurrence of a surface relaxation might be a general feature of lyotropic mesophases consisting of regularly arranged micelles in water. However, although the experiments on the H_1 phase of $C_{12}E_5$/water are well reproducible, it is not clear whether the observed effect occurs generally. Another question which is still to be answered is how the surface relaxation is related to the shift of the phase transition temperature reported earlier.[11] Both questions are subject of our current research and will be adressed in forthcoming papers.

Acknowledgment. The authors thank A. Möller and U. Menge for their help with the experiments and Prof. U. Pietsch from the University of Potsdam for helpful discussions. Thanks are due to the staff at HASYLAB for ample beam time and support. This work was supported by the Deutsche Forschungsgemeinschaft (Sonderforschungsbereich 335, "Anisotrope Fluide").

References and Notes

(1) Dietrich, S., Findenegg, G. H., Freyland W., Eds. *Ber. Bunsen-Ges. Phys. Chem.* **1994**, *98*, 279.
(2) Dosch, H. *Critical Phenomena at Surfaces and Interfaces*; Springer Tracts in Modern Physics 126; Springer: Berlin, 1992.
(3) Ocko, B. M.; Braslau, A.; Pershan, P. S.; Als-Nielsen, J.; Deutsch, M. *Phys. Rev. Lett.* **1986**, *57*, 94. Kellogg, G. J.; Pershan, P. S.; Kawamoto, E. H.; Foster, W.; Deutsch, M.; Ocko, B. M. *Phys. Rev. E* **1995**, *51*, 4709.
(4) Earnshaw, J. C.; Hughes, C. J. *Phys. Rev. A* **1992**, *46*, 4494.
(5) Ocko, B. M.; Wu, X. Z.; Sirota, E. B.; Sinha, S. K.; Gang, O.; Deutsch, M. *Phys. Rev. E* **1997**, *55*, 3164.
(6) Deutsch, M.; Wu, X. Z.; Sirota, E. B.; Sinha, S. K.; Ocko, B. M.; Magnussen, O. M. *Europhys. Lett.* **1995**, *30*, 283.
(7) Mitchell, D. J.; Tiddy, G. J. T.; Waring, L.; Bostock, T.; MacDonald, M. P. *J. Chem. Soc., Faraday Trans. 1* **1983**, *79*, 975.
(8) Sjöblom, J.; Stenius, P.; Danielsson, I. In *Nonionic Surfactants Physical Chemistry*; Schick, M. J., Ed.; Surfactant Science Series 23; Marcel Dekker: New York, 1987.
(9) Glatter, O.; Strey, R.; Schubert, K. V.; Kaler, E. *Ber. Bunsen-Ges. Phys. Chem.* **1996**, *100*, 323.
(10) Strey, R.; Schomäcker, R.; Roux, D.; Nallet, F.; Olsson, U. *J. Chem. Soc., Faraday Trans. 1* **1990**, *86*, 2253.
(11) Braun, Chr.; Lang, P.; Findenegg, G. H. *Langmuir* **1995**, *11*, 764.
(12) Zhou, X. L.; Lee, L. T.; Chen, S. H.; Strey, R. *Phys. Rev. A* **1992**, *46*, 6479.
(13) Als-Nielsen, J.; Kjær, K. In *Phase Transitions in Soft Condensed Matter*; Riste, T., Sherrington, D., Eds.; Plenum Press: New York, 1989.
(14) Marra, W. C.; Eisenberger, P.; Cho, A. Y. *J. Appl. Phys* **1979**, *50*, 6927.
(15) Eisenberger, P.; Marra, W. C. *Phys. Rev. Lett.* **1981**, *46*, 1091.
(16) Braslau, A.; Deutsch, M.; Pershan, P. S.; Als-Nielsen, J.; Bohr, J. *Phys. Rev. Lett.* **1985**, *54*, 114.
(17) Salditt, T.; Rhan, H.; Metzger, H.; Peisl, J.; Kotthaus, J. P. *Z. Phys. B* **1994**, *96*, 227.
(18) Tanford, C. *The Hydrophobic Effect*; Wiley: New York, 1973.